Journal of Power Sources 227 (2013) 41–47

Contents lists available at SciVerse ScienceDirect

Journal of Power Sources

journal homepage: www.elsevier.com/locate/jpowsour

Development of carbon coated membrane for zinc/bromine flow battery with high power density

Liqun Zhang [a,b], Huamin Zhang [a,*], Qinzhi Lai [a], Xianfeng Li [a], Yuanhui Cheng [a,b]

[a] Division of Energy Storage, Dalian Institute of Chemical Physics, Chinese Academy of Sciences, 457 Zhongshan Road, Dalian 116023, China
[b] Graduate School of the Chinese Academy of Sciences, Beijing 100039, China

HIGHLIGHTS

- A carbon coated membrane (CCM) is first developed and employed for the zinc/bromine flow battery.
- A distinguished improvement of the activity of the positive electrode is achieved.
- The internal resistance of the cell decreases obviously attributed to CCM.
- High energy efficiency of 75% is achieved which increases by 68% at 40 mA cm^{-2}.
- A nearly two-fold increase in the power density is achieved.

ARTICLE INFO

Article history:
Received 10 July 2012
Received in revised form
24 September 2012
Accepted 12 November 2012
Available online 20 November 2012

Keywords:
Carbon
Energy storage
Zinc/bromine flow battery
Power density

ABSTRACT

The zinc/bromine flow battery is considered as one of the most suitable candidates for the large-scale electrical energy storage attributed to its nature of high energy density and low cost. However, the relatively low power density determined by the working current density of 20 mA cm^{-2} limits its performance and application. The relatively low working current density is caused by the insufficient electrochemical activity of positive electrode and the high internal resistance of cell. The formation of Br_{ads} is the rate-determined step to the positive electrode reaction. Thus the activated carbon with the specific surface area of 2314 m^2 g^{-1}, compared with the carbon felt, is a much more suitable and competitive choice. The activated carbon coated membrane is first designed to decrease the internal resistance. Demonstrated by the cycle voltammetry, AC impedance and polarization distribution investigations, both the positive electrode overpotential and the cell internal resistance decrease obviously attributed to the high electrochemical activity layer closing to the membrane. Thus the energy efficiency of 75% is achieved at charge–discharge current density of 40 mA cm^{-2}, which means a nearly two-fold increase in power density.

1. Introduction

It is necessary to develop large-scale electrical energy storage for the grid to meet the demand on the integration of renewable energy sources and the construction of smart grid [1]. The redox flow battery (RFB) is considered as one of the most suitable and promising candidates for large-scale electrical energy storage [2,3]. Based on the redox couples employed, the RFBs include: iron/chromium (Fe/Cr) flow battery [4], bromine/polysulphide flow battery (PSB) [5], vanadium flow battery (VFB) [6–8] and zinc/bromine flow battery (ZBB) [9]. The Br_2/Br^- redox couple is employed in the positive electrode of ZBB based on the following reaction:

$$2Br^- \Leftrightarrow Br_2 + 2e^- \ (E^\theta = 1.07 \text{ V vs. SHE})$$

And the Zn^{2+}/Zn redox couple is employed in the negative electrode:

$$Zn^{2+} + 2e^- \Leftrightarrow Zn \ (E^\theta = -0.76 \text{ V vs. SHE})$$

Compared with the other candidates, the ZBB exhibits higher energy density and lower cost [10]. However, the power density of ZBB determined by the product of working current density and cell voltage is too low for the high power-rate application. Moreover, the advantage of low cost for ZBB has been weakened by the large number of single cell needed for a battery module. The insufficient

* Corresponding author. Tel.: +86 411 84379072; fax: +86 411 84665057.
E-mail address: zhanghm@dicp.ac.cn (H. Zhang).

0378-7753/$ – see front matter © 2012 Elsevier B.V. All rights reserved.
http://dx.doi.org/10.1016/j.jpowsour.2012.11.033

power density is caused by the relatively low working current density of 20 mA cm^{-2} due to the high reaction polarization of the positive electrode and the internal resistance of the cell.

In order to raise the power density, it is necessary to develop the electrode material possessing high activity to the Br_2/Br^- redox couple and design the low internal resistance cell. The carbon nanotube is proposed to produce the positive electrode [11], while it is too expensive to be used in the large-scale energy storage. The activated carbon with affordable cost exhibits comparatively high activity and reversibility to the positive electrode reaction [12]. Thus the activated carbon is used in the positive electrode of the ZBB. In order to improve the utilization of the activated carbon electrode, the carbon coated membrane (CCM) is first developed and employed in the ZBB. Moreover, the electrochemical reaction sites are concentrated in the activated carbon layer which is closed to the membrane. As a result, the ionic transport distance is shortened and the internal resistance of the cell is reduced attributed to the CCM. Thus the cell employed CCM is project to work at higher current density. And the improvement of the power density will be achieved.

The physicochemical properties of the activated carbon and carbon felt are explored by scanning electron microscope (SEM) and N_2 adsorption/desorption isotherms. The electrochemical activity and interfacial resistance of them are investigated by the cycle voltammetry and AC impedance measurements, respectively. The in-situ electrochemical measurements are carried out to the cell employed CCM to prove the improvement of the electrochemical activity of positive electrode. The distribution of the polarization is demonstrated by the measurements of the half-cell potential and IR drop across membrane during charge–discharge cycling at 20 mA cm^{-2} and 40 mA cm^{-2}, respectively.

2. Experimental

2.1. Characterization of carbon materials

The morphology of the carbon materials were characterized by a QUANTA 200F scanning electron microscope (SEM) operated at 20 kV. The specific surface area (S_{BET}) and pore size distribution were analyzed by nitrogen adsorption/desorption isotherms at 77 K on an Automated Surface Area and Pore Size Analyzer (QUADRASORB SI). In order to investigate the electrochemical properties, the cyclic voltammetry and AC impedance tests were employed using a three-electrode cell controlled by a Soltron electrochemistry workstation. The electrolyte was composed of 2 M $ZnBr_2$ and 0.05 M N-methylethylpyrrolidinium bromide (MEPB) [13]. A glassy carbon disk electrode (d = 4 mm) coated with carbon powders, a piece of graphite plate (2 cm × 2 cm) and a saturated calomel electrode (0.244 V vs. SHE) were used as working electrode, counter electrode and reference electrode, respectively. The working electrode was prepared by dripping 10 μl of carbon powder ink onto the pre-polished GC disk electrode. The ink was made by dispersing 5 mg carbon materials (carbon felt powder and activated carbon powder) and 20 μl of 0.05 wt% Nafion solution in 1 ml isopropanol under a strong ultrasonication.

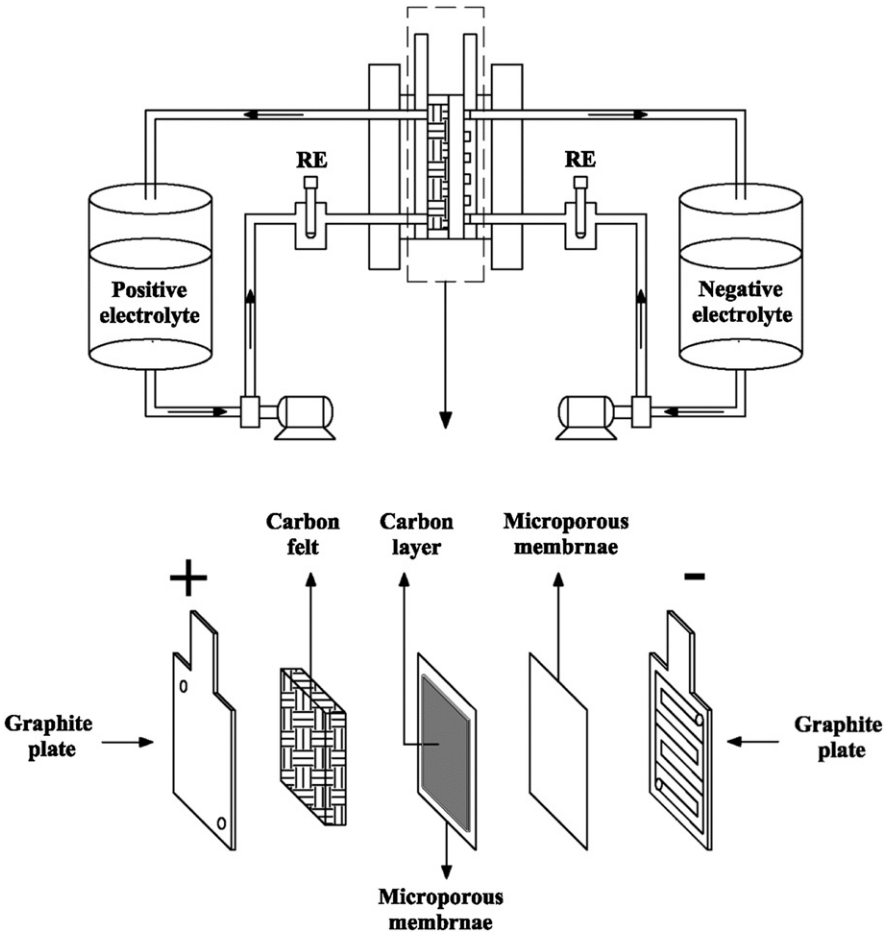

Fig. 1. Schematic diagram of the zinc/bromine flow battery employed carbon coated membrane (CCM).

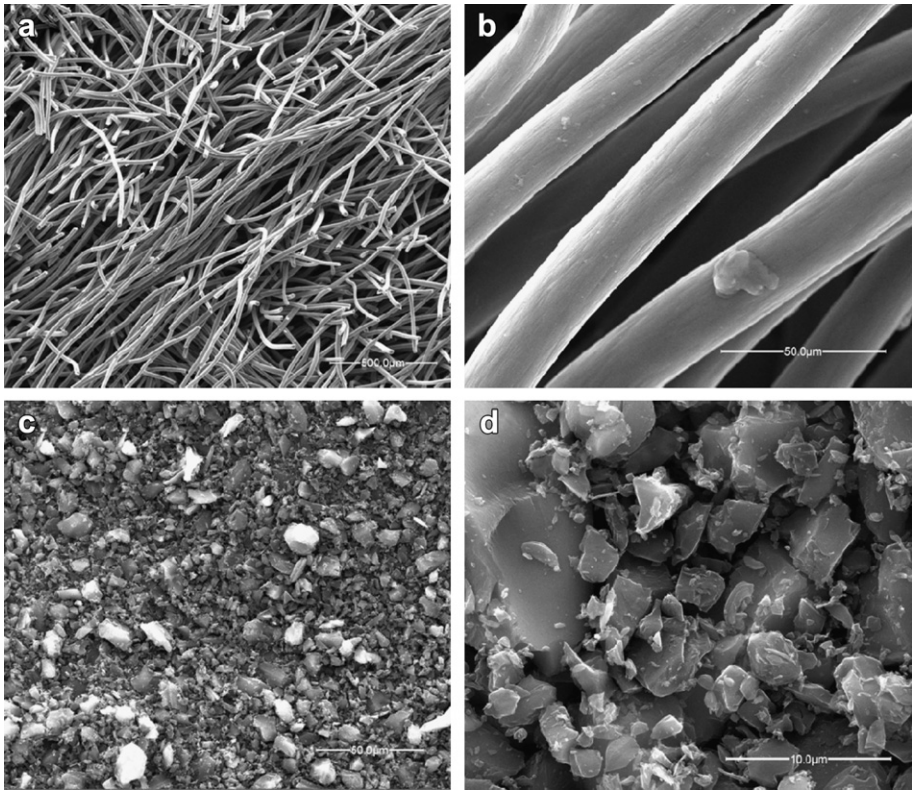

Fig. 2. SEM images of carbon felt (a, b) and activated carbon (c, d).

2.2. Preparation of carbon coated membrane (CCM)

A piece of Daramic® microporous membrane with a thickness of 200 μm was used as the substrate for carbon coating. The activated carbon layer was prepared by spraying carbon ink onto the surface of microporous membrane with loading of 5 mg cm^{-2}. The carbon ink was made by dispersing activated carbon and 0.05 wt% Nafion solution based on the desired ratios in ethanol under a strong ultrasonication. At last the CCM was dried at 70 °C for 4 h.

2.3. Characterization of the CCM

The cross-sectional morphology of the CCM was observed by scanning electron microscope (JSM-6360LV, JEOL). The in-situ cyclic voltammetry tests were employed to the zinc/bromine flow cell by a potentiostat (CHI 612C) to investigate the activity and reversibility of the positive electrode based on the CCM. The positive and negative electrodes were used as working electrode and counter electrode, respectively. The saturated calomel electrode (SCE) inserting in the positive electrolyte circuit was used as reference electrode. The in-situ AC impedance measurements were carried out by means of two-electrode connections controlled by Kikusui KFM 2030 FC impedance meter with sweeping frequencies over the range from 1 Hz to 10 kHz at the open circuit voltage.

2.4. Zinc/bromine flow cell charge–discharge cycling test

The schematic diagram of the cell with electrode area of 36 cm^2 (6 cm × 6 cm) is presented in Fig. 1. The cell employed CCM was assembled by sandwiching CCM and a piece of microporous membrane between carbon felt and negative graphite plate. A piece of microporous membrane was employed instead of CCM in the cell employed conventional electrode. The graphite plate with flow channel was used as the substrate for zinc deposition. The positive and negative electrolytes were composed of 2 M $ZnBr_2$ and 0.05 M N-methylethylpyrrolidinium bromide (MEPB). The MEPB was used to capture bromine molecules and store as the form of polybromide complexes. Both of them were stored in their respective tanks and pumped into the corresponding compartments during charge–discharge cycling test. The saturated calomel electrode (SCE) connecting into each half-cell electrolyte circuit was used as reference electrode (RE) to continuously monitor the positive and negative electrode potentials and IR drop across the membrane. The area capacity was fixed at 20 mAh cm^{-2}, so the charge time was 1 h at 20 mA cm^{-2} and 0.5 h at 40 mA cm^{-2}. The discharge process continued until the cell voltage dropped below 0.5 V.

3. Results and discussion

The representative SEM images of the carbon felt are presented in Fig. 2(a) and (b). The carbon felt is composed of the carbon fiber with the diameter of ~17 μm. Based on the nitrogen adsorption/desorption isotherms results (summarized in Table 1), there is few pore structure in the carbon felt. Thus the specific BET area is determined by the external surface area of ~0.632 m^2 g^{-1}. As shown in Fig. 2(c) and (d), the activated carbon shows obviously different morphology. The powder size of the activated carbon distributes from 2 μm to10 μm. The external surface area of

Table 1
Parameters on specific surface and pore structure.

Sample	S_{BET} (m^2 g^{-1})	$S_{External}$(m^2 g^{-1})	V_p (cm^3 g^{-1})	D_p (nm)
Carbon felt	0.632	0.632	NA	NA
Activated carbon	2314	43.65	1.128	1.95

activated carbon increases to 43.65 $m^2\ g^{-1}$ attributed to the decrease of the powder size. The specific BET area increases to 2314 $m^2\ g^{-1}$, most of which is contributed by the micro-pores whose average pore diameter is ~1.95 nm.

The rate determined steps of the Br^- oxidation reaction and Br_2 reduction reaction are proposed as following [14]:

Br^- oxidation reaction:

$$Br^- \rightarrow Br_{ads} + e^-$$

Br_2 reduction reaction:

$$Br_2 + e^- \rightarrow Br_{ads} + Br^-$$

Both of them are determined by the chemical adsorption process. Thus the activated carbon possessing high specific surface area and strong adsorption ability is project to exhibit sufficient high electrochemical activity. In order to clarify the activated carbon is a better candidate, the cycle voltammetry tests are carried out over the range from 0.244 V to 1.144 V versus the standard hydrogen electrode (SHE) at the scan rate of 20 mV s^{-1}. As shown in Fig. 3, the anodic current is attributed to the Br^- oxidation reaction and the cathodic current peak is attributed to the Br_2 reduction reaction. There is no anodic current peak observed during the positive scan. It results from the sluggish oxidation reaction rate and the high Br^- concentration. The anodic current of activated carbon is much higher than that of carbon felt at the same potential. At the reverse potential (1.144 V), the anodic current of activated carbon is ~9.3 mA, while that of carbon felt is ~2 mA. The potential of cathodic current peak of activated carbon is around 0.9 V with current of ~6.8 mA, while that of carbon felt is around 0.9 V with current of 0.8 mA. The results demonstrate the activated carbon possesses higher specific electrochemical activity. However, the superiority of the electrochemical activity is not as significant as that of the specific surface area. It mainly results from the following factors: first, the utilization of the surface area is limited by the non- accessible micro-pores; second, the high reaction activity sites are occupied by the production such as Br_2 in the oxidation reaction and Br^- in the reduction reaction.

The AC impedance tests are employed from 1 Hz to 3×10^5 Hz at the potential of 0.994 V (vs. SHE) based on the same three-electrode cell. The Nyquist plots of the carbon materials are shown in Fig. 4. In the high-frequency section (activated carbon: 1.2×10^4 Hz–3×10^5 Hz; carbon felt: 1.2×10^5 Hz–3×10^5 Hz), the condensance

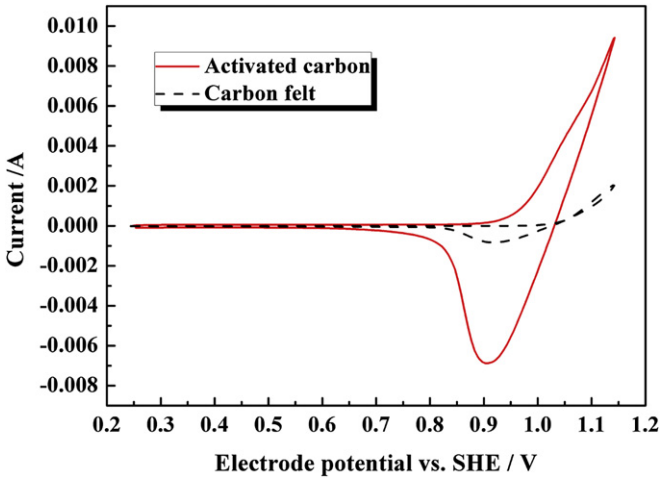

Fig. 3. Cyclic voltammograms of the activated carbon and carbon felt with a scan rate of 20 mV s^{-1} at 25 °C.

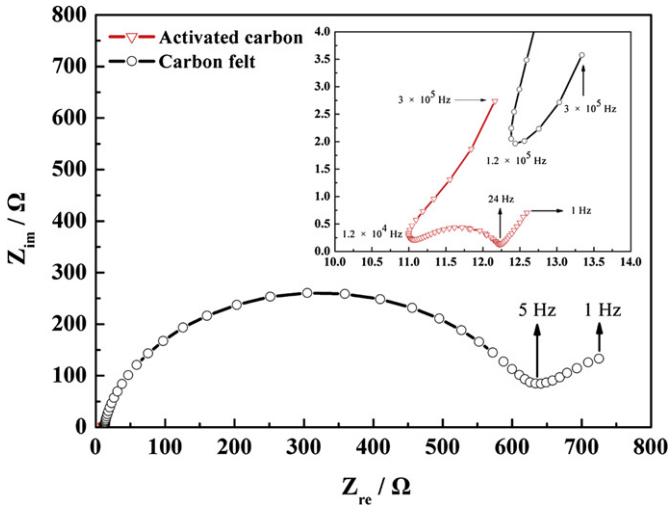

Fig. 4. Nyquist plots of the activated carbon and carbon felt from 1 Hz to 3×10^5 Hz at 0.994 V vs. SHE.

which is determined by the $(2\pi f C)^{-1}$ drops with the decrease of the frequency (f). It indicates the electrochemical double layer capacitance (C) of the carbon materials increases dramatically. It results from the increase of the chemisorption of Br^- ions caused by the AC signal. The mid-frequency arc is corresponding to the charge-transfer process of the positive electrode reaction. The carbon felt exhibits much bigger arc radius, which implies the sluggish charge-transfer rate. Although affected by the electrochemical double-layer, the interfacial resistance can be obtained by extension the mid-frequency arc. The interfacial resistance of the activated carbon is about 11.0 Ω, while that of the carbon felt is about 12.3 Ω. The lower interfacial resistance of activated carbon is caused by the much larger electrode/electrolyte interface. In the low-frequency section (activated carbon: 1–24 Hz; carbon felt: 1–5 Hz), the Warburg resistance is observed. It indicates that the reaction rate is partly determined by the diffusion process. Most of the electrochemical activity sites of activated carbon distributes in the internal surface. Thus the mass transfer resistance increases due to the narrow pore size. Although the electrochemical activity sites of carbon felt distributes in the external surface, the limited surface area is partly occupied by the absorbed Br^- and Br_2. Thus the mass transfer resistance increases due to the site exclusion effect.

The SEM image of the cross-sectional morphology of CCM is presented in Fig. 5. As shown in the photograph, the carbon layer tightly adheres to the surface of microporous membrane with the thickness of about 5 μm. And there is no obvious boundary between the carbon layer and microporous membrane attributed to the similarity between Nafion resin and microporous membrane. Thus the CCM exhibits high mechanical stability during the charge–discharge cycling test.

The in-situ cycle voltammetry tests are carried out to the positive electrode employed CCM and carbon felt respectively in the potential window from 0.244 V to 1.144 V (vs. SHE) at the scan rate of 30 mV s^{-1}. As shown in Fig. 6, the anodic current of the electrode employed CCM is 0.125 A at 1.144 V, while that of the electrode employed carbon felt is 0.069 A. The cathodic current peak of the electrode employed CCM is observed at 0.72 V with current of 0.095 A, while that of the electrode employed carbon felt is observed at 0.7 V with current of 0.058 A. It indicates the electrochemical activity of the positive electrode employed CCM is superior to the conventional electrode. However, the superiority is not as remarkable as the specific activity investigation. It results from the increase of electrochemical active surface based on the flow-

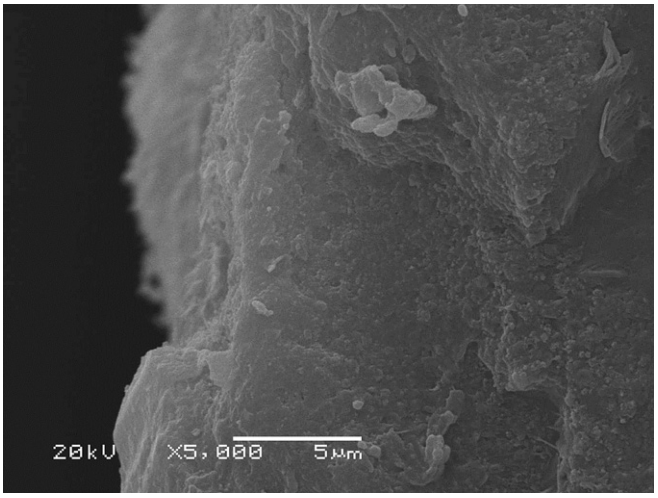

Fig. 5. SEM micrograph of the cross-sectional of carbon coated membrane (CCM).

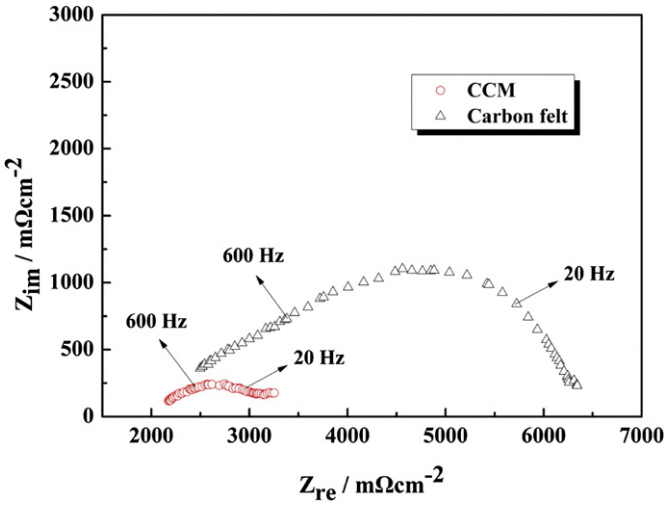

Fig. 7. Impedance spectra of the cell employed CCM and carbon felt at the open circuit voltage.

through electrode. In the potential window without Br_2/Br^- redox reaction, the electrochemical double layer charge–discharge current of the electrode employed CCM increases dramatically. It is attributed to the increase of double layer capacitor producing by the activated carbon.

The AC impedance measurements are carried out to the cell having been charged for 1 h at 20 mA cm^{-2}. As shown in Fig. 7, there are two impedance arcs in the Nyquist plot. The high-frequency arc ranging from 10 kHz to 600 Hz is corresponding to the charge-transfer process of the negative electrode reaction and the low frequency arc ranging from 600 Hz to 20 Hz is corresponding to the charge-transfer process of the positive electrode reaction. The radius of the arc reflects the charge-transfer resistance, and the smaller arc radius implies the faster reaction rate. There is a negligible difference in the high frequency part of the Nyquist plot since the same negative electrodes are employed. However, the radius of the low-frequency arc decreases obviously to the cell employed CCM. It indicates the electrochemical activity of the positive electrode increases based on the CCM.

The charge–discharge curve for the cell employed CCM and carbon felt at the current density of 20 mA cm^{-2} is presented in Fig. 8(a). The charge voltage of the cell employed CCM is about 1.77 V at the beginning and increases to 1.85 V, while the charge voltage plateau of the cell employed carbon felt is 1.88 V. The positive half-cell potential of the cell employed CCM is 0.99 V initially and increases to 1.04 V since the absorbed Br_2 prevents Br^- adsorption due to site exclusion. The positive half-cell potential of

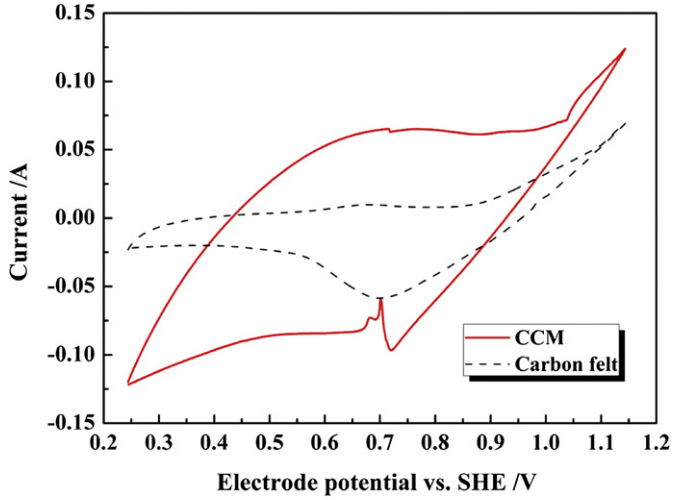

Fig. 6. Cyclic voltammograms of the positive electrode employed CCM and carbon felt with a scan rate of 30 mV s^{-1} at 25 °C.

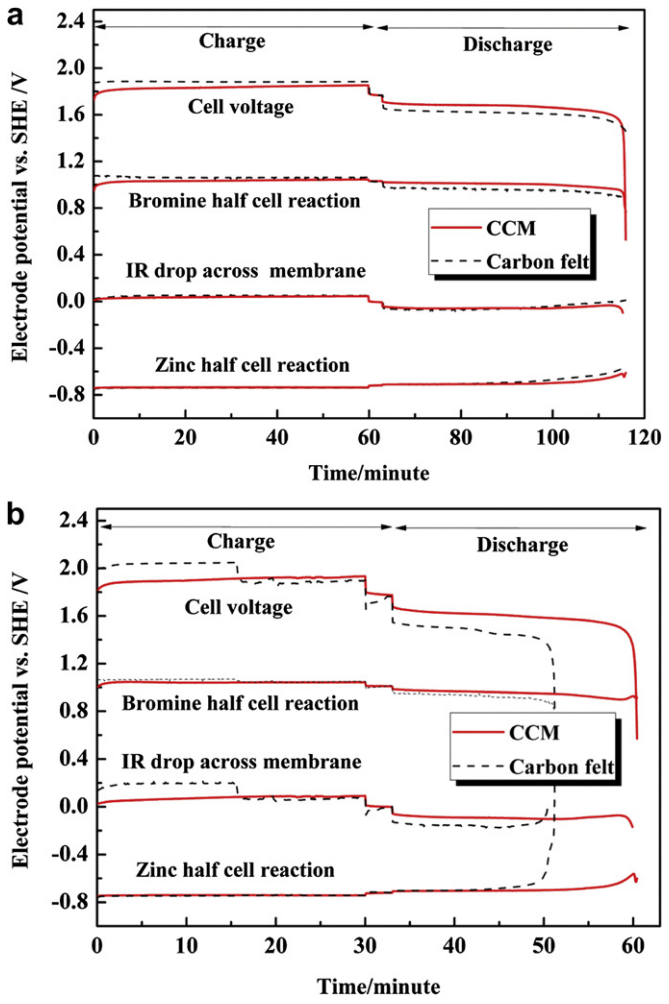

Fig. 8. Voltage vs. time characteristics of the zinc/bromine flow battery employed CCM and carbon felt for a full charge–discharge cycle: (a) 20 mA cm^{-2}, (b) 40 mA cm^{-2}.

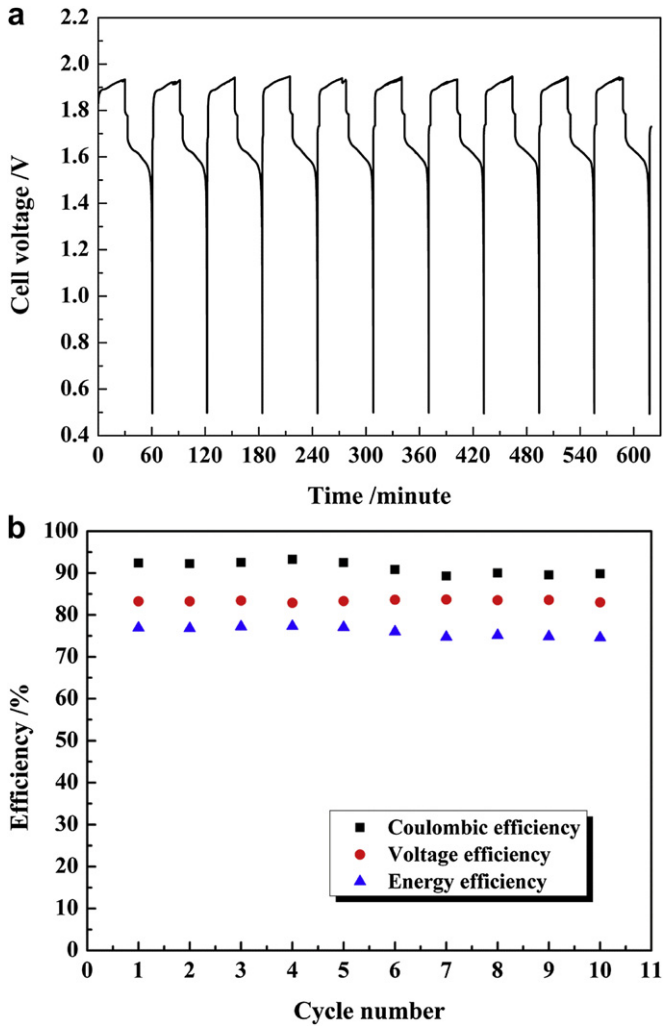

Fig. 9. Life cycle of the zinc/bromine flow battery employed CCM working at 40 mA cm^{-2}.

the cell employed carbon felt is 1.08 V. Thus the fall of the charge voltage of the cell employed CCM is mainly caused by the decrease of the polarization of the positive electrode. The discharge voltage plateau of the cell employed CCM is 1.68 V, while that of the cell employed carbon felt is 1.62 V. The raise of discharge voltage plateau is attributed to the decrease of the overpotential of the positive electrode whose potential increases from 0.96 V to 1.01 V attributed to the CCM. Thus the voltage efficiency of the cell employed CCM increases to 90.7%, while that of cell employed carbon felt is 84.8%. And the energy efficiency of the cell employed CCM increases from 73.2% to 80.3%.

The voltage versus time plot obtained for a full charge–discharge cycle at 40 mA cm^{-2} is shown in Fig. 8(b). The charge voltage of the cell employed CCM rises from 1.85 V to 1.93 V, while that of the cell employed carbon felt is 2 V at the beginning and drops to 1.9 V. The IR drop across membrane of the cell employed CCM is about 70 mV at 40 mA cm^{-2}, which is nearly twice of that at 20 mA cm^{-2}. The voltage drop versus current relation obeys Ohm's law since the local reaction rate is mainly distributed within the activated carbon layer. However, the initial IR drop across membrane of the cell employed carbon felt is 150 mV at 40 mA cm^{-2}, while it is only 30 mV at 20 mA cm^{-2}. It indicates that the ionic transport process becomes more difficult and complicate due to the reaction site distribution expands vertically within the carbon felt when the charge current increases [15]. During the cell employed carbon felt charging at 40 mA cm^{-2}, the Br_2 molecules are accumulated in the microporous membrane. Due to the following chemical equilibrium in the membrane and electrode boundary, the transport rates of the Br^- and Br_2 increase.

$$Br^- + Br_2 \Leftrightarrow Br_3^-$$

As a result, the IR drop across membrane of the cell employed carbon felt decreases to 70 mV. And the coulombic efficiency drops to 60.7%, while that of the cell employed CCM is 91.5%. The Br_2 molecules stored in the membrane are desorbed and removed during the standing and discharge operation, which leads to the IR drop across membrane returns to 160 mV. However, the IR drop across membrane of the cell employed CCM is 90 mV during discharge. And the positive half-cell potential of the cell employed CCM increases from 0.94 V to 0.97 V. Thus the discharge voltage plateau increases from 1.5 V to 1.6 V. Based on the accumulation of the voltage–time plot, the voltage efficiency increases from 74.9% to 83.5%. And the energy efficiency of 76.4% is achieved, which is 30% higher than that of cell employed conventional electrode.

The 40 mA cm^{-2} charge–discharge cycling performance of the cell employed CCM is presented in Fig. 9. There is a negligible difference in the cell voltage versus time plot among the every charge–discharge cycle. It demonstrates that the CCM exhibits acceptable stability and reliability. The coulombic efficiency of 91 ± 1% and the voltage efficiency of 83 ± 0.5% are obtained, respectively. And the energy efficiency of 76 ± 1% is achieved. It is even higher than that of the cell employed conventional electrode working at 20 mA cm^{-2}. Thus the cell employed CCM is able to work at 40 mA cm^{-2} and the two-fold increase in the power density is realized.

4. Conclusions

The formation of the absorbed intermediate (Br_{ads}) is rate-determined step to the positive electrode reaction. Thus the activated carbon with high specific surface area and strong adsorption ability is a suitable material to be employed as the positive electrode of ZBB. The internal resistance of the cell decreases obviously attributed to the construction of a high electrochemical activity layer closing to the membrane. Based on the increase of positive electrode activity and the decrease of internal resistance, the energy efficiency of cell employed CCM increases from 73.2% to 80.3% during charge–discharge at 20 mA cm^{-2}. More importantly, the energy efficiency of 75% is achieved during charge–discharge at 40 mA cm^{-2}. Compared with the cell employed conventional electrode, the energy efficiency increases by 68%. As a result, the power density of the ZBB nearly doubles and the cost almost reduces by half. For purpose of improving the cycling life at high current density, the further investigation and optimization of the CCM is being carried out in our lab.

Acknowledgment

This work was financially supported by the National Basic Research Program of China (973 program No. 2010CB227204)

References

[1] Bruce Dunn, Haresh Kamath, Jean-Marie Tarascon, Science 334 (2011) 928–935.
[2] Z.G. Yang, J.L. Zhang, Michael C.W. Kintner-Meyer, X.C. Lu, Daiwon Choi, J.P. Lemmon, J. Liu, Chem. Rev. 111 (2011) 3577–3613.
[3] C. Ponce de León, A. Frías-Ferrer, J. González-García, D.A. Szánto, F.C. Walsh, J. Power Sources 160 (2006) 716–732.
[4] L.H. Thaller, Electrically Rechargeable Redox Flow Cells. NASA TM-X-71540 (1974).
[5] H.T. Zhou, H.M. Zhang, P. Zhao, B.L. Yi, Electrochim. Acta 51 (2006) 6304.

[6] M. Skyllas-Kazacos, M. Rychcik, R.G. Robins, A.G. Fane, M.A. Green, J. Electrochem. Soc. 133 (1986) 1057–1058.
[7] P. Zhao, H.M. Zhang, H.T. Zhou, B.L. Yi, Electrochim. Acta 51 (2005) 1091.
[8] M. Skyllas-Kazacos, George Kazacos, Grace Poon, Hugh Verseema, Int. J. Energy Res. 34 (2010) 182–189.
[9] P.C. Butler, P.A. Eidler, P.G. Grimes, S.E. Klassen, R.C. Miles, Zinc/Bromine Batteries, in: D. Linden, T.B. Reddy (Eds.), Handbook of Batteries, McGrawHill, 2001, pp. 39.1–39.20.
[10] Liqun Zhang, Qinzhi Lai, Jianlu Zhang, Huamin Zhang, ChemSusChem 5 (2012) 867–869.
[11] Yuyan Shao, Mark Engelhard, Yuehe Lin, Electrochem. Commun. 11 (2009) 2064–2067.
[12] Phillip Eidler, Development of Zinc/Bromine Batteries for Load-Leveling Applications: Phase 1 Final Report. Sandia report, SAND99–1853 (1999).
[13] Krystyna Cedzynska, Electrochim. Acta 40 (1995) 971–976.
[14] Marina Matragostino, Carla Gramellini, Electrochim. Acta 30 (1984) 373–380.
[15] Kuo-Chuan Ho, Jacob Jorne, J. Electrochem. Soc. 133 (1986) 1394–1398.